Synergistic strengthening by nano-sized α-Al(Mn,Fe)Si and Al_3Zr dispersoids in a heat-resistant Al-Mn-Fe-Si-Zr alloy

Shiwei Pan[1,2], Feng Qian[2,3], Chunan Li[2], Jiawei Yang[2], Zidong Wang[1], Yanjun Li[2*]

[1] State Key Laboratory for Advanced Metals and Materials, University of Science and Technology Beijing, Beijing 100083, China

[2] Department of Materials Science and Engineering, Norwegian University of Science and Technology, 7491, Trondheim, Norway

[3] School of Materials Science and Engineering, Beijing Institute of Technology, Beijing, 100081, China

Abstract: Strengthening by dispersoids in Al alloys has been limited by either low number density or low volume fractions of dispersoids. In the present work, the influence of an addition of 0.28wt% Zr on precipitation hardening behavior of AA3003 alloy subjected to different heat treatments has been investigated. A superior microstructure simultaneously consisting of nano-sized α-Al(Mn,Fe)Si and Al_3Zr dispersoids at peak-aged state was achieved by two different heat treatment regimes, ramp heating with a speed of 50°C/h and isothermal aging at 400°C. As a result, a substantial increase in yield strength of 30MPa (43%) was achieved in comparison to AA3003 alloy. Meanwhile, the 3003-Zr alloy exhibits excellent heat-resistance with a stable yield strength from 12h (106MPa) up to 250h (107MPa) during isothermal aging at 400°C. This remarkable thermal stability was ascribed to the continuously hardening from Al_3Zr precipitation, which compensates the strength loss from α-dispersoid

coarsening. Besides, TEM study shows that the precipitation kinetics of Al_3Zr is significantly enhanced compared with the reference binary Al-Zr alloy, which is attributed to the Si content in the alloy. This work proposes an effective method to design a low-cost heat-resistant Al alloy in mass production.

Keywords: Aluminum alloy; α-dispersoid; Al_3Zr; Precipitation; Diffusivity

* Corresponding authors:

E-mail address: yanjun.li@ntnu.no

1. Introduction

Age hardening is one of the most effective strengthening methods for aluminum alloys[1]. The conventional age-hardened alloys, such as 2xxx ,6xxx and 7xxx series, are generally strengthened by precipitates formed at temperature lower than 250°C[2,3]. However, these age-hardening precipitates are metastable and coarsen rapidly with increasing temperature (>250°C), which results in dramatical strength loss[4]. In contrast to this, dispersoids precipitated at higher temperatures like Al_3Zr, Al_3Sc and α-Al(Mn,Fe)Si, are more stable and can be utilized as strengthening phases in Al alloys for the purpose of elevated temperature applications (>300°C) as automotive/aerospace structural components[5–9]. More specifically, the high thermal stability of dispersoids usually arises from the slow diffusivities of the dispersoid-forming elements (e.g. Mn, Zr, Nb, Sc, Cr, Fe and Mo) in Al matrix, which causes a slow coarsening kinetics at elevated temperatures[6,10–12]. However, like two sides of the same coin, the sluggish thermal-induced diffusion also leads to a long aging time required to reach the peak-aged state. Furthermore, most of the alloys are suffered from low number density and low volume fraction of dispersoids[9]. Therefore, it is still necessary to explore new approaches to achieve a better dispersion strengthening effect of dispersoids in Al alloys.

α-Al(Mn,Fe)Si is the dominant dispersoid precipitated in commercial AA3xxx (Al–Mn–Fe–Si) alloys and some Mn-bearing 5xxx and 6xxx series alloys, which is mainly used for texture modification[13–15]. It has a cubic crystal structure (Pm3) with a lattice parameter of 1.256-1.265 nm, and the orientation relationships between the partially coherent α-dispersoid and the Al matrix have been well defined in our previous

reports[14,16,17]. Most of α-dispersoids in AA3xxx alloys incline to decompose from the supersaturated solid solution and nucleate on dislocations within the aging temperature range of 350-450°C, thus leading to a relatively low number density, large size and heterogeneous distribution [13]. As a result, α-dispersoids were usually regarded to have a negligible strengthening effect in 3xxx Al alloys. In the past decade, various methods including chemical composition modification[18], heat-treatment regime optimization[14,19] and microalloying[20], have been applied to modify the precipitation behavior and therefore improve the dispersion hardening effect of α-dispersoid. Nevertheless, the improvements in mechanical strength are still limited.

Al_3Zr dispersoid, which presents low coarsening kinetics and high stability at temperatures up to ~0.7Tm (melting temperature of alloy) of Al, ~400°C[21–23], is a widely used strengthening phase in heat-resistant Al alloys. Unfortunately, Al-Zr binary alloy hardly produces a significant precipitation hardening effect due to the insufficient diffusivity of Zr [24]. One of the mostly applied methods to solve this problem is micro-alloying with various elements, such as Sc, Er, Y, Yb and Si[25–29], to accelerate the precipitation kinetics in Al-Zr based alloys. However, the hardening effect is still highly restricted by the low volume fraction (<0.5%) of the $L1_2$-strctured dispersoids since Zr and other related elements have rather limited solubilities in the Al matrix[9].

Recently, some research efforts have been made to improve mechanical properties by introducing two distinct populations of particles. For instance, it is reported that both of 50-70nm-sized α-Al(Mn,Fe)Si and 6-8nm-sized $Al_3(Sc,Zr)$ dispersoids can contribute to mechanical performance in a 3004 alloy with addition of Sc and Zr[5]. A

hardness increment (ΔHV) of ~10 was obtained during isothermal aging. Although with two kinds of dispersoids, the dispersion hardening effect is less significant than the corresponding Al-Sc-Zr alloy. De Luca et. al. designed a novel heat-resistant Al-Zr-Sc-Er-Si alloy with Mn and Mo addition, which exhibits a fast-aging response as well as a slow coarsening rate[30–32]. In this case, the strength contribution mostly arises from the Mn, Mo solute atoms and Sc-containing $L1_2$ nanoparticles, while the micro-sized α-dispersoids (>100nm) have negligible contribution to the mechanical strength.

Since Sc is an extremely expensive rare-earth (RE) element, addition of Sc entails significant costs. From this viewpoint, it is interesting to investigate whether nanoscale α-dispersoids and $L1_2$ Al_3Zr particles can be simultaneously utilized as strengthening phases in a RE-free Al alloy by delicate composition and heat-treatment optimization. If possible, this can serve as an effective method to design a low-cost and heat-resistant Al alloy for mass production.

In the present study, a commercial AA3003 alloy is chosen as the base alloy to investigate the precipitation behavior with and without Zr micro-addition. The design philosophy of this composition is to form high density dispersodis of both nano-sized α-Al(Mn,Fe)Si and Al_3Zr phases upon aging. Precipitation of strengthening dispersoids in 3003-Zr alloy during ramp heating until 600ºC was investigated in comparison with the reference 3003 and Al-Zr alloys. In addition, thermal stability of the dispersoids at 400ºC was comprehended with the combination of electron microscopy and mechanical tensile tests.

2. Experiments and methods

A commercial DC-cast AA3003 extrusion ingot (with addition of Al5Ti1B grain refiner) supplied by Hydro Inc. was used as the raw material and melted in a crucible furnace. Zr was added into the melt in form of master alloy (Al-6wt.% Zr) at 800ºC, holding for 1h with regular stirring. After degassed by high purity argon gas, the liquid melt was cast in a copper mold to obtain an ingot with a dimension of 25*70*100 mm^3. For reference, a binary Al-Zr alloy and a remelted 3003 ingot were cast at 800ºC and 750ºC, respectively. Chemical compositions of all as-cast alloys determined by X-ray Fluorescence Spectrometer (XRF) technique are presented in Table 1.

Table 1. Chemical compositions of the as-cast alloys (wt. %).

	Al	Mn	Fe	Si	Zr
3003	Bal	1.08	0.56	0.20	-
3003-Zr	Bal	0.97	0.53	0.18	0.28
Al-Zr	Bal	-	-		0.28

Two regimes of heat-treatment were applied on as-cast samples: 1. ramp heating with a heating rate of 50 ºC /h was performed from RT up to 600 ºC, followed water quenching one after another at different temperatures; 2. Samples were firstly ramp-heated to 400ºC with a rate of 50 ºC /h, and then isothermal aged at the same temperature until 250h. Vickers hardness tests were performed on polished specimens at different aged states, using a 500 g load and 10s dwell time. Ten indentations across the same sample surface were tested for each sample. Electrical conductivity values were measured by a Foerster *Sigmatest 2.069* eddy current instrument for each sample utilizing frequencies of 60, 120, 240, 480, and 960 kHz. Dog-bone shaped specimens (a gauge length 30 mm and 6 mm × 2 mm in cross section) were machined according

to ASTM standard[33] and tensile tests were carried out at room temperature using a strain rate of 1×10^{-3}s. Three tensile tests were conducted for each aging-state to ensure the replicability of results.

A *Zeiss Axio* optical microscope (OM) was used for the observation of grain structures in the as-cast samples after grinding, polishing and further anodizing with 95 wt.% H_2O +5 wt.%HBF_4 solution at 20V for 90s. A *Zeiss Ultra* field-emission SEM equipped with energy dispersive spectroscopy (EDS) was utilized to characterize primary phases as well as the fractography of tensile samples, while BSE mode was used to investigate the distribution of dispersoids. Thin foils for TEM observation were prepared by electro-polishing procedure in an electrolyte of 30% HNO_3 in methanol at -25 ºC. *JEOL 2010/2100* TEMs were operated at 200 kV for bright/dark field imaging and selected area electron diffraction (SAED). The average sizes of dispersoids were determined by measuring >200 particles from TEM images by means of *Image J* software.

3. Results

3.1 As-cast microstructure

Fig. 1 shows the typical grain structure of as-cast 3003 and 3003-Zr alloys. The reference 3003 alloy shows a fine and fully equiaxed grain structure with an average grain size of 187μm. In contrast, the 3003-Zr alloy exhibits a coarse columnar grain structure with an average grain size of >800μm. This is ascribed to the "poisoning effect" of Zr atoms on Al-Ti-B grain refiners, which is identical with that reported in literatures[34,35]. In addition, Fig. 1b and d reveal that the secondary dendrite arms are

finer in 3003 than that in 3003-Zr. It could be explained by the cooling rate effect during solidification due to the different casting temperatures for 3003 (750 °C) and 3003-Zr (800 °C) alloys. Furthermore, some pores, from dozens of microns to hundreds of microns range, are identified in 3003-Zr microstructure. This could be induced by the severe absorption of gas during the high temperature (800°C) melting process.

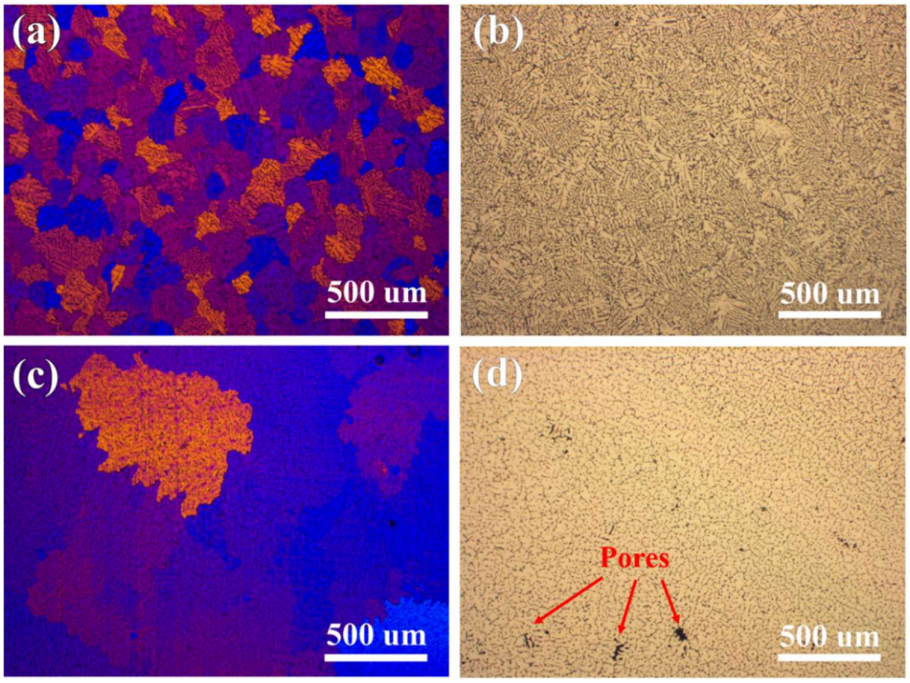

Fig. 1. Optical micrographs of the as-cast (a,b) 3003 and (c,d) 3003-Zr alloys. Note (a,c) are polarized light optical macrographs while (b,d) are bright-field images, respectively.

Fig. 2 presents the morphology of the Fe, Mn-rich constituent particles in the as-cast 3003-Zr alloy characterized by SEM with corresponding EDS mapping results. As can be seen in Fig. 2a, the constituent particles of skeletal shape mainly distribute in the inter-dendritic regions, and most of them have been identified as Al_6(Mn,Fe) phase by EDS. This is a common constituent phase with orthorhombic crystal structure presented in 3xxx alloys with low Si content[36]. Besides, a small amount of plate-like α-Al(Mn,Fe)Si particles can be observed, as depicted in Fig. 2b. Interestingly, a local

enrichment of Zr can be detected in some of the α-Al(Mn,Fe)Si particles. It seems that the formation of Zr-rich particles favors the precipitation of the cubic structured α-$Al_{15}(Mn,Fe)_3Si_2$ intermetallic phase during solidification.

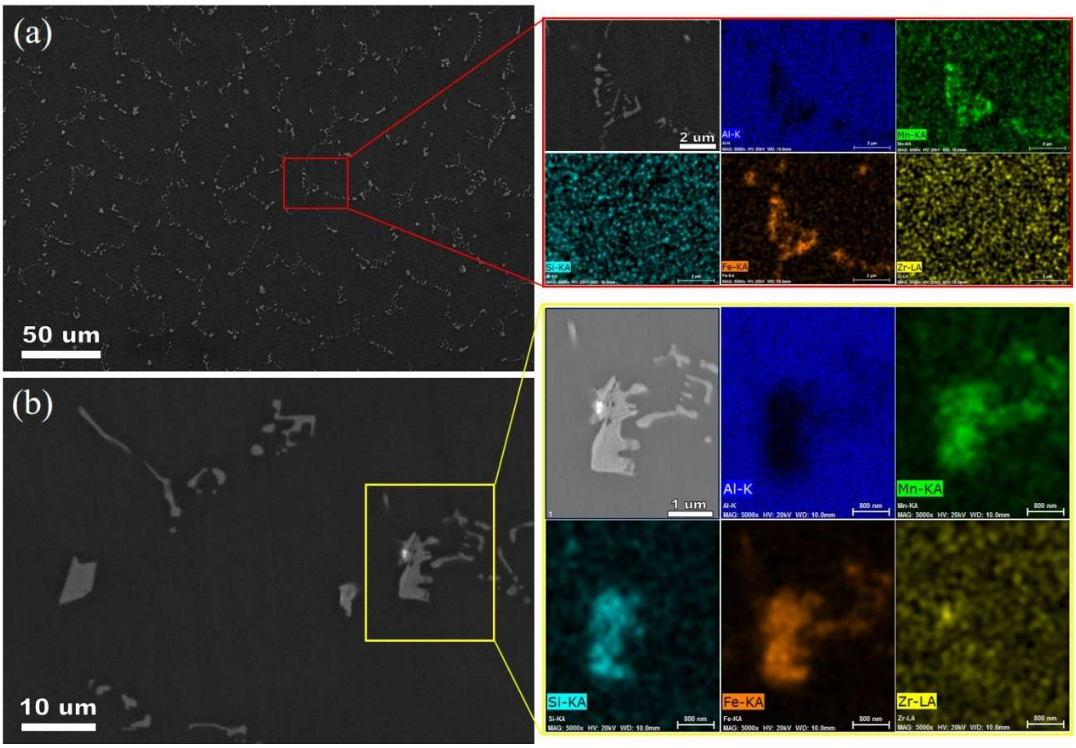

Fig. 2. SEM-BSE micrographs with different magnifications of the as-cast 3003-Zr alloy. Insets on the right are enlarged images and EDS mapping of primary $Al_6(Mn,Fe)$ phase and $Al_{15}(Fe,Mn)_3Si_2$ phase formed during solidification in (a) and (b), respectively. Note the compositions of the constituent particles were identified by EDS point scanning but not shown here.

3.2 Ramp heating from RT to 600°C

3.2.1 Microhardness and electrical conductivity evolution

Fig. 3 shows the temporal evolutions of Vickers microhardness (HV) and electrical conductivity (EC) of the investigated alloys during ramp heating. In the as-cast state, there is a considerable amount of Mn and Zr solute atoms existed in the Al matrix, which strongly influences the hardness and EC values. As a result, 3003-Zr has the highest hardness but lowest EC among the three as-cast alloys. During ramp heating,

both 3003 and Al-Zr binary alloy display rather limited age-hardening, obtaining maximum increase in hardness of 3.8 and 5.5 HV at the peak-aged state of 450°C and 500°C, respectively. In contrast, 3003-Zr displays a superior age-hardening behavior with a faster kinetics and a higher peak hardness value. More specifically, the hardness of 3003-Zr starts to rise from 300°C, followed by a sharp increase observed at 350°C, and then continues to grow until 450ºC, reaching a peak value of 60.5. As a result, a total hardness increment of 12.2 HV has been obtained, which is more than the sum of the hardness increase values in 3003 and Al-Zr alloys. With t further increasing of temperature, the microhardness of both 3003 and 3003-Zr alloys turns to decrease, which is related to the coarsening/dissolution of the hardening phase.

As seen in Fig. 3, the evolution of EC curves is consistent with that of the hardness evolution. The EC of Al-Zr remains almost stable until 400ºC, and reaches a peak value at 500ºC, suggesting a sluggish precipitation kinetics. For 3003 alloy, the EC starts to increase from 350ºC and obtain a peak value at 450ºC, then it changes to decrease with heating to higher temperatures. In comparison, 3003-Zr alloy demonstrates a similar trend of EC evolution but faster kinetics than 3003 reference alloy. An early precipitation of dispersoids commencing at 300 ºC with a subtle EC increment of 0.4MS/m can be detected in 3003-Zr alloy. After that EC gradually increases and reaches to the peak at 500ºC. It is worth of noting that EC increment of about 0.7MS/m during the range of 450-500ºC can still be obtained, which indicates a further decomposition of the supersaturated solid solution and precipitation of dispersoids. Finally, the fast decrease of EC beyond 500 ºC indicates the dissolving of dispersoids

in the alloy.

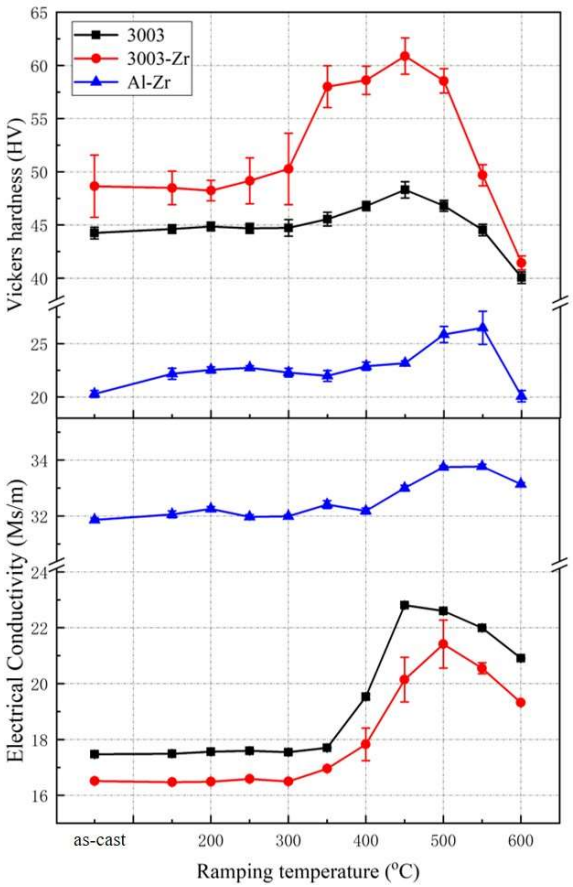

Fig. 3. Temporal evolution of the Vickers microhardness and electrical conductivity at room temperature, during ramp heating aging with heating rate of 50 ºC /h for 3003, 3003-0.28Zr and Al-0.28Zr (wt. %) alloys. The increase of EC is an indication of the precipitation of α-Al(Mn,Fe)Si and/or Al_3Zr while a decrease of EC means the dissolution of dispersoids.

3.2.2 Dispersoids at peak-aged state

Dispersoids precipitated in the experimental alloys at the peak-aged state during ramp heating (450 ºC for 3003 and 3003-Zr, 500 ºC for Al-Zr) were characterized by TEM, and representative images as well as the measured size distribution are shown in Fig. 4 and Fig. 5, respectively. It should be mentioned that all the presented images for each alloy are taken from the areas with high density dispersoids. In 3003 alloy, a large amount of blocky and platelet-shaped α-Al(Mn,Fe)Si dispersoids can be observed (Fig.

4a and b). The average equivalent diameter was measured as 38.9nm. It seems that α-dispersoids have precipitated preferentially along some lines, which can be ascribed to heterogeneous nucleation along dislocation lines in the Al matrix (Fig. 4b). For Al-Zr binary alloy, there is a high density of Al_3Zr dispersoids in the center region of dendrite arms, which have spherical shape and a mean radius of 4.9nm, as seen in Fig. 4c, d and Fig. 5b. Meanwhile, the superlattice spots in the corresponding selected area diffraction pattern (SADP) demonstrate that Al_3Zr particles have $L1_2$ structure (inset in Fig. 4c).

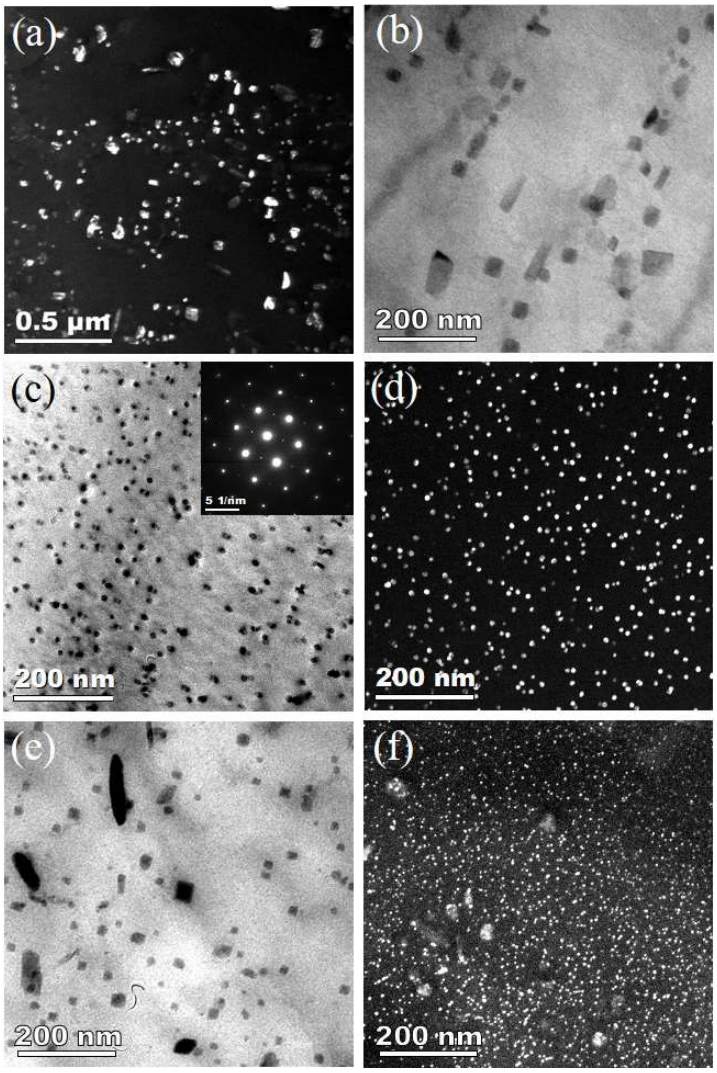

Fig. 4. TEM images of the peak-aged (a, b) 3003, (c, d) Al-Zr and (e, f) 3003-Zr alloys during ramp heating. Note the presented images for 3003 and Al-Zr alloys are taken from dendrite periphery and

center, respectively. For 3003-Zr alloy, the bright-field image (e) is taken within the dense α zone, while the dark-field image (f) is taken within the dendrite center region with the densest distribution of Al_3Zr dispersoids.

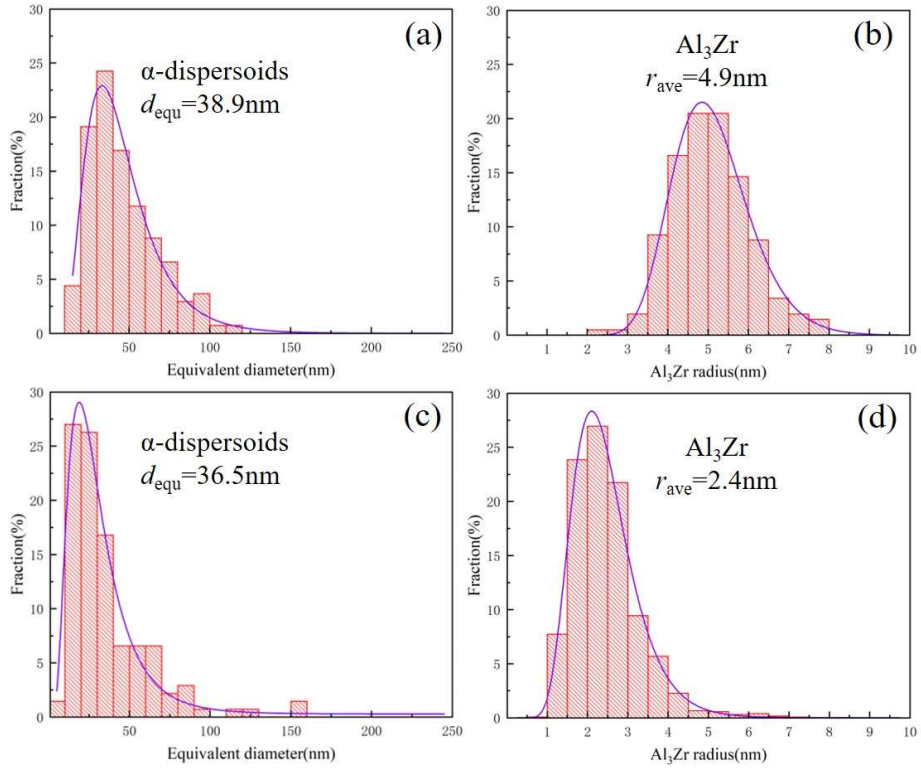

Fig. 5. Respective size distribution histograms of the α dispersoids and Al_3Zr nanoparticles in the peak-aged (a) 3003, (b) Al-Zr and (c) 3003-Zr alloys. The distributions exhibit a log-normal shape. Note d_{equ} and r_{ave} in the figures stand for the mean equivalent diameter of α dispersoids and the average radius of Al_3Zr, respectively.

In 3003-Zr alloy, it is interesting to see from Fig. 4 e and f that both nano sized α-Al(Mn,Fe)Si and Al_3Zr dispersoids have precipitated after ramp heating to 450 °C. Compared with the reference alloys, morphologies of both types of dispersoids barely changed. However, as shown in Fig. 4e, the Al_3Zr dispersoids has a much higher density and a much smaller size than those in the binary Al-Zr alloy. The size distribution profiles in Fig. 5 also confirms that the Al_3Zr dispersoids in 3003-Zr alloy show a narrower size distribution and about half average size as Al-Zr alloy.

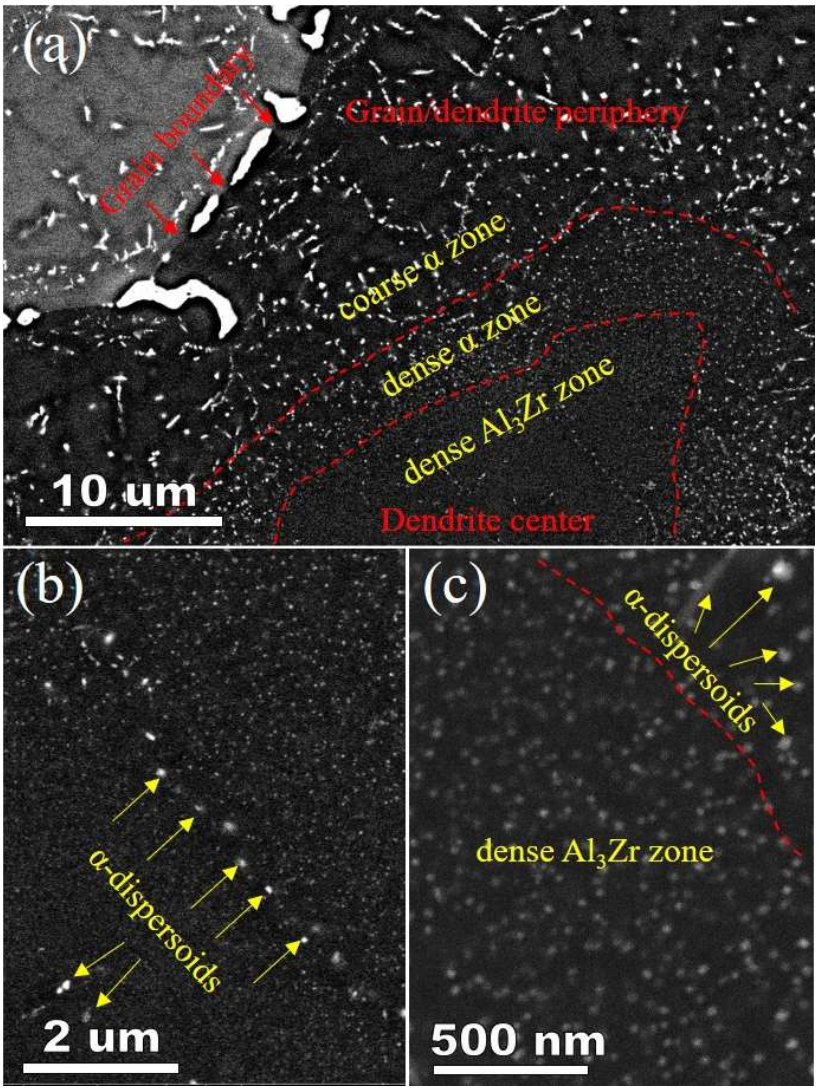

Fig. 6. SEM-BSE images of the peak-aged 3003-Zr alloy after ramping to 450°C. (a) Low-magnification micrograph shows the distribution of two types of dispersoids from the grain/dendrite periphery to the dendrite center, (b) some spherical α-dispersoids detected in the dendrite center area and distributed closely proximity as a line, (c) high-magnification micrograph of the transition region from the dense α zone to the dendrite center (dense Al_3Zr Zone).

To characterize the distribution of dispersoids across dendrite arms in the peak-aged 3003-Zr alloy, SEM-BSE images were taken. . As shown in Fig. 6a, three different regions can be distinguished from the dendrite periphery to the dendrite center, namely coarse α zone, dense α zone and dense Al_3Zr zone. In coarse α zone, α-Al(Mn,Fe)Si (d_{equ}>200nm) is the dominant dispersoid while the density of Al_3Zr is very low. In this zone, the size of α dispersoids gradually increases towards the grain boundary. As can

be seen, the dispersoids-free zones (DFZ) around the grain boundary are very narrow. Dense Al_3Zr zone is located in the dendrite center, where most of the particles are determined as Al_3Zr and only a small fraction of them are identified as α phase (Fig. 6b), which is consistent with the TEM image shown in Fig. 4f. In between the dense Al_3Zr zone and coarse α zone there is a narrow dense α zone. In this region, both α and Al_3Zr dispersoids can be observed, and the α dispersoids are finer and denser than in coarse α zone. Fig.6c shows a clear transition from the dense Al_3Zr zone to the dense α zone. It is clear that α-Al(Mn,Fe)Si and Al_3Zr show an opposite distribution trend in terms of number density. This should be ascribed to the different segregation behaviors of Mn and Zr during solidification process, where Mn, as a eutectic element, is enriched in the inter-dendritic region, while Zr, as a peritectic element, has an enrichment in dendrite center during solidification. The depletion of Mn in the center of dendrite arms is more serious for coarse dendrite arms, which has also been observed in a AA3103 alloy[36].

3.3 Isothermal aging after ramp heating to 400°C

3.3.1 Microhardness and electrical conductivity evolution

The evolution of Vickers hardness and electrical conductivity for the investigated alloys during isothermal aging after ramp-heating to 400°C is presented in Fig. 7. The hardness of 3003-Zr increases slowly with heating time and reaches a peak value after 12h. After that, the microhardness value slowly drops from 59.3 to 58.6 HV after 250h aging, indicating the 3003-Zr alloy is very stable at 400°C. In contrast, 3003 alloy shows a monotonic decrease from 48.2 HV at 1h to 40.9 HV at 250h, showing a massive loss

of strengthening effect from the dispersoids. For Al-Zr binary alloys, it shows a continuous and slow hardness increase with aging time. After 250h aging, a microhardness of 26.4 HV is achieved.

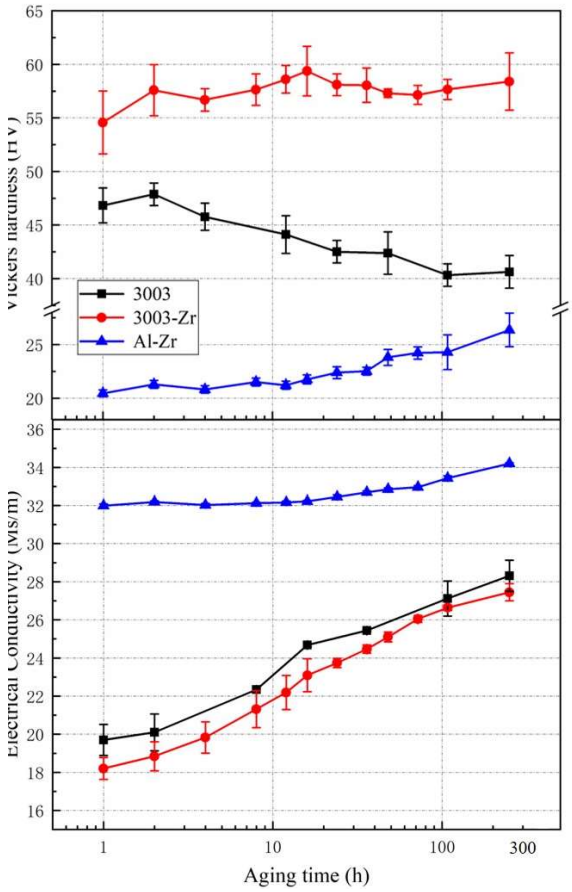

Fig. 7. Temporal evolution of the Vickers microhardness and electrical conductivity of 3003, 3003-0.28Zr and Al-0.28Zr (wt. %) alloys during isothermal aging after ramp heating from RT to 400°C with a rate of 50°C/h. To minimize the systematic error, all the data for each alloy were collected on the same sample with various aging time.

As seen in Fig. 7, the monotonic increase of EC from the beginning of aging in 3003 and 3003-Zr alloy indicates a continuous decomposition of supersaturated solid solution. The total electric conductivity increase, ΔEC, of the two alloys are 4.1 and 4.7 Ms/m, respectively. However, a faster increase of EC in 3003-Zr can be found between 12h and 108h compared with that in 3003, thus suggesting a more significant precipitation during this period. In contrast, the evolution of EC in Al-Zr alloy is quite

slow with a ΔEC of ~1 Ms/m after aging for 250h.

3.3.2 Evolution of dispersoids

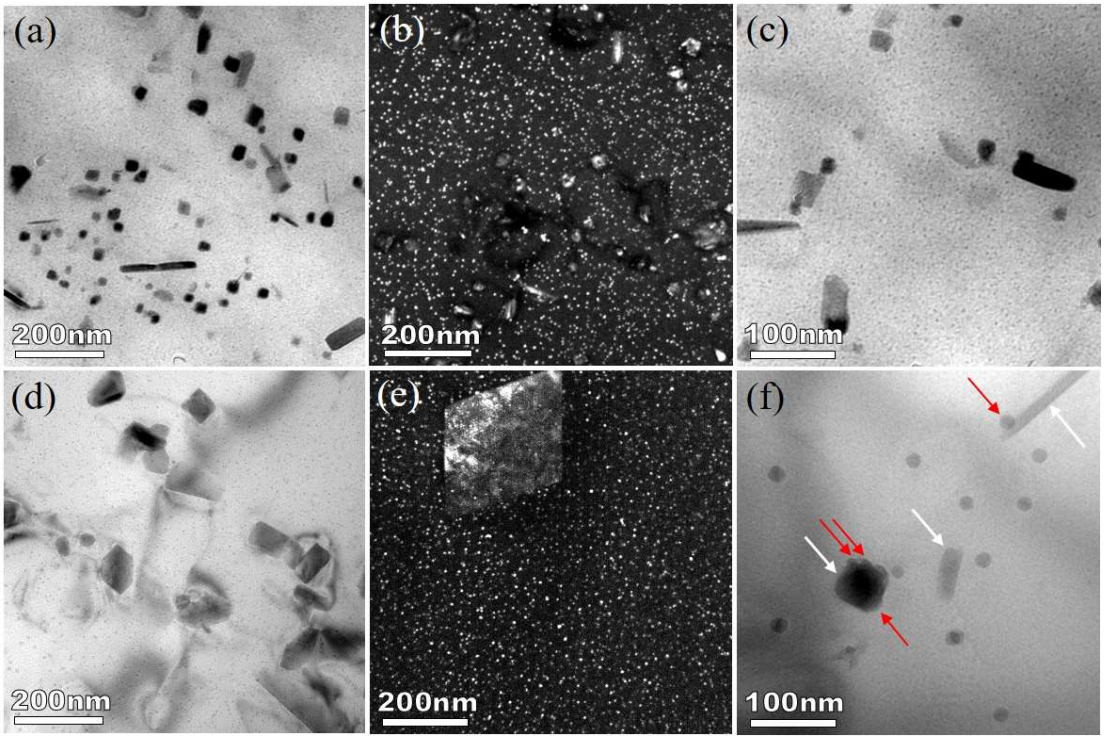

Fig. 8. TEM images of the 3003-Zr alloy after isothermal aging at 400°C for (a-c) 12h and (d-f) 250h, respectively. (a, b, d, f) are taken from dendrite periphery regions with dense α-dispersoids, while (c, e) are taken from dense Al_3Zr zone in dendrite center. (f) shows heterogeneous nucleation of Al_3Zr (pointed by red arrows) on α-dispersoids (white arrows).

TEM micrographs of 3003-Zr alloy after isothermal aging for 12h and 250h are shown in Fig. 8 and the corresponding size distributions of the dispersoids are displayed in Fig. 9. After 12h-aging, there are dense and fine α-dispersoids in dendrite periphery regions and dispersed Al_3Zr nanoparticles (Fig. 8a and b), while the dendrite center region is dominated by a higher density of finer Al_3Zr dispersoids and has a sparse distribution of α-dispersoids (Fig. 8c). As shown in Fig. 9a and b, the sizes of α-dispersoids and Al_3Zr after 12h aging at 400°C are similar to that obtained at peak-aged state (Fig. 5c and d). After 250h aging, α-dispersoids show a dramatic increase in size to 86nm (Fig. 9c). In this case, the number density of α-dispersoids dramatically

decreases accompanied with the interparticle spacing increasing as shown in Fig. 8d. Meanwhile, Al_3Zr dispersoids only show a small increase in size from 2.8 to 3.1nm (Fig. 9d), indicating that Al_3Zr is more resistant to coarsening than α-dispersoids at elevated temperature. Fig. 8f demonstrates that some Al_3Zr dispersoids are clearly attached to the surface of α-dispersoids, suggesting a possible heterogeneous nucleation of the Al_3Zr on α-dispersoids. However, this phenomenon is hardly seen in the dendrite center.

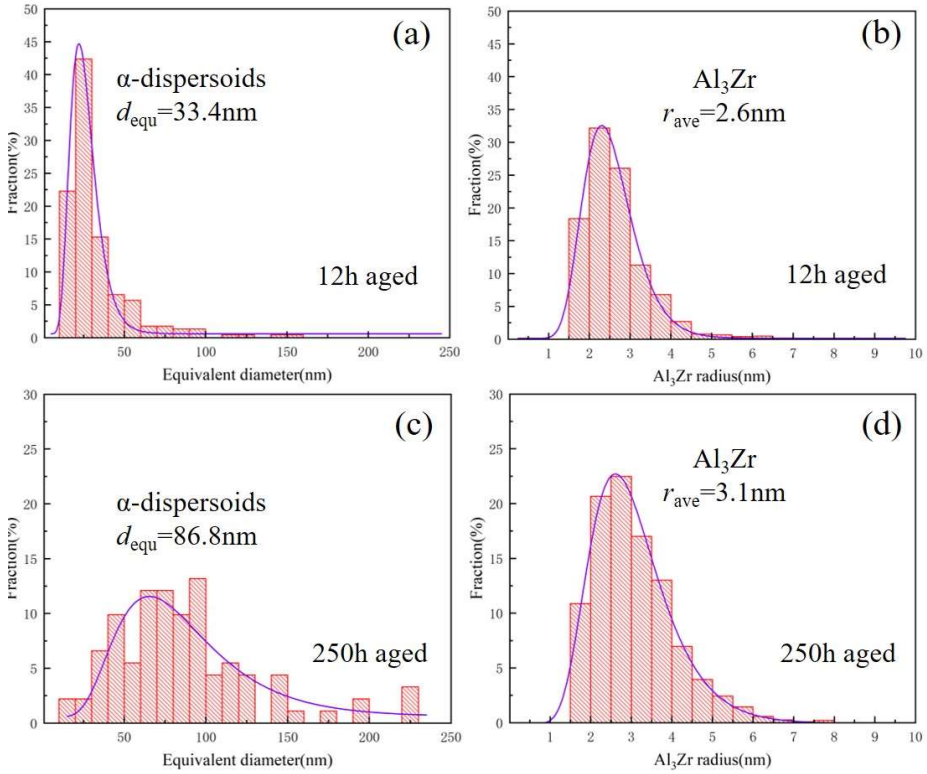

Fig. 9. Respective size distribution histograms of the α-dispersoids and Al_3Zr nanoparticles of the 3003-Zr alloy after aging at 400°C for (a,b) 12h and (c,d) 250h, respectively.

3.4 Tensile properties

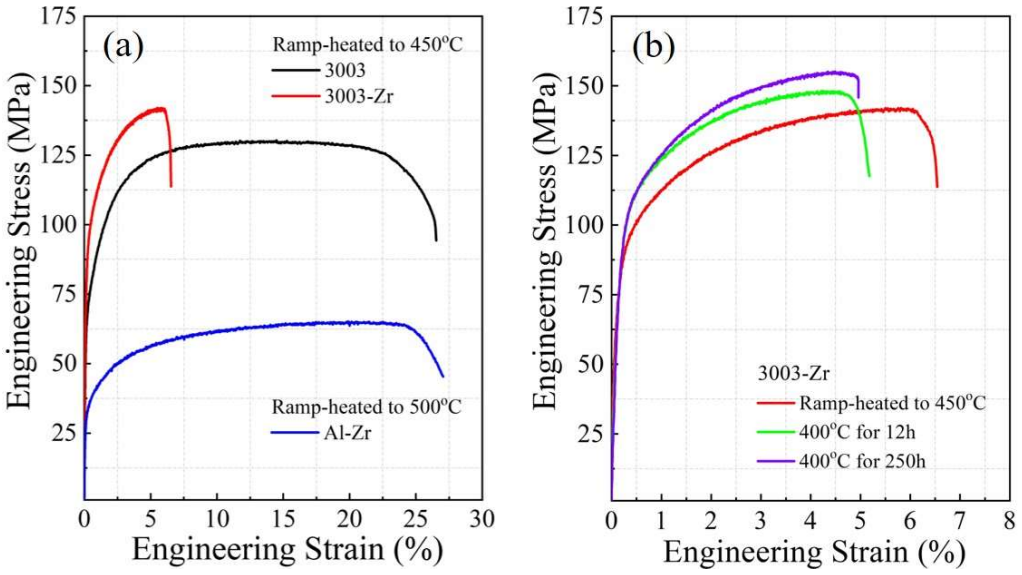

Fig. 10. Tensile stress-strain curves for (a) all investigated alloys after ramp-heated to their peak-aged state, and (b) the 3003-Zr alloy after ramp-heating to 400 °C and then isothermal aging for 12h and 250h, respectively. Note the tensile curve of 3003-Zr as-heated to 450 °C is also displayed in (b) as a reference. (For interpretation of the references to color in this figure legend, the reader is referred to the Web version of this article.)

Engineering stress-strain curves of all studied alloys subjected to different heat treatments are presented in Fig. 10, and the corresponding yield strength, ultimate strength and elongation derived from tensile curves are summarized in Table 2. As can be seen in Fig. 10a, the peak aged 3003-Zr alloy (as-heated to 450 °C) has the highest yield strength of 99MPa among all studied alloys, which is corresponding to an improvement of 30MPa (43%) compared with the 3003 alloy. Based on the microstructure observation, this increment value mainly arises from the Al_3Zr dispersoids, which is obviously higher than that of the Al-Zr binary alloy (23MPa). In addition, it should be noted that 3003-Zr show an elongation value of 6%, much lower than 3003 alloy. This discrepancy is of course partially associated with a trade-off between strength and ductility which is common in precipitation-strengthening alloys[37]. It should also be related to the casting porosities in 3003-Zr produced during

solidification, as seen in Fig. 1d. SEM images of the fractography in Fig. 11 exhibits a typical ductile fracture pattern with micron-sized shallow dimples, indicating an insufficient ductility. Several big pores (larger than 100um) can also be observed in the fracture surface, which may induce stress concentration and initiation of early cracks.

Table 2. Tensile yield strength, ultimate strength and elongation of studied alloys at different states.

State	Alloy	Yield Strength /MPa	Ultimate Strength /MPa	Elongation /%
Ramp-heated to 450 °C	3003	69 ± 2	128 ± 2	25.9 ± 2.1
	3003-Zr	99 ± 5	147 ± 1	6 ± 1.2
Ramp-heated to 500 °C	Al-Zr	36 ± 3	65 ± 2	27 ± 4
400°C for 12h	3003-Zr	106 ± 1	154 ± 3	4.6 ± 1.6
400°C for 250h		107 ± 1	155 ± 1	5.7 ± 0.9

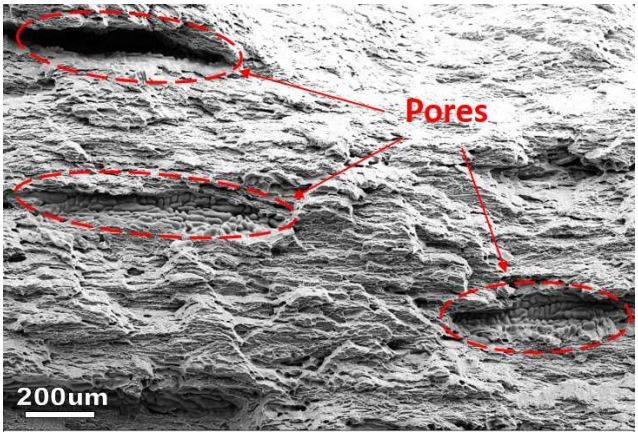

Fig. 11. SEM micrograph of fracture surface of tested peak-aged 3003-Zr after ramp heating to 450°C.

Fig. 10b displays the mechanical performance of 3003-Zr after ramp-heating to 400°C and then isothermal aging for 12h and 250h. The yield strength (106MPa) and ultimate strength (154MPa) of the 12h-aged sample are higher than those of peak-aged samples by ramp heating, although the microstructures are similar. After long time aging for 250h, no obvious change in the yield strength, ultimate strength and elongation can be detected which is consistent with the hardness results in section 3.3.1.

It demonstrates that 3003-Zr has a high thermal stability when exposed to 400 ºC for a long time, which is mainly attributed to the fine Al_3Zr instead of α-dispersoids (Fig. 8d-e).

4. Discussion

4.1 Precipitation behavior of dispersoids during ramp-heating

In the present study, it shows that a microstructure containing high density nano-sized dispersoids of both Al_3Zr and α-Al(Mn,Fe)Si can be achieved in commercial AA3003 alloy, by addition of Zr combined with appropriate aging regimes. Generally, the nucleation, growth and coarsening of dispersoids are closely related to diffusivity of the dispersoid-forming elements. As shown in Fig. 12, the diffusion of Zr in Al matrix at temperatures below 350ºC is extremely slow, $D_{Zr}<10^{-21}m^2/s$, resulting in negligible diffusion distance during this temperature range. In comparison, the diffusivity of Mn is about two orders of magnitude higher than Zr between 300ºC and 400ºC. It is known that α-Al(Mn,Fe)Si dispersoids usually start to precipitate at temperature above 300ºC[20]. Thus the distinct change in hardness and electrical conductivity at 350ºC is supposed to be due to the precipitation of α-Al(Mn,Fe)Si dispersoids. With the temperature increasing, the hardness increment of 3003-Zr at 400ºC and 450ºC is much higher than that of the reference 3003 alloy, implying that the precipitation of Al_3Zr dispersoids has started from 400ºC. This is different from Al-Zr binary alloy, for which distinct hardness increment can only by observed at 500ºC, indicating that the precipitation of Al_3Zr dispersoids in 3003-Zr alloy is much faster. This accelerated precipitation kinetics of Al_3Zr is likely due to the Si content in 3003 alloy. It has been

reported that Si has the influence of promoting the precipitation of Al_3Zr dispersoids in Al-Zr series alloys[27,38]. Different from 3003 alloy, there is still an obvious increment of electrical conductivity value of 3003-Zr alloy form 450°C to 500°C, which indicates a further precipitation and growth of Al_3Zr particles. In the meantime, the decrease in hardness in this temperature range is due to the rapid coarsening and dissolution of α-dispersoids. Finally, rapid coarsening and dissolution of both dispersoids inevitably dominates the process beyond 500 °C, as indicated by the EC decreasing in Fig. 3.

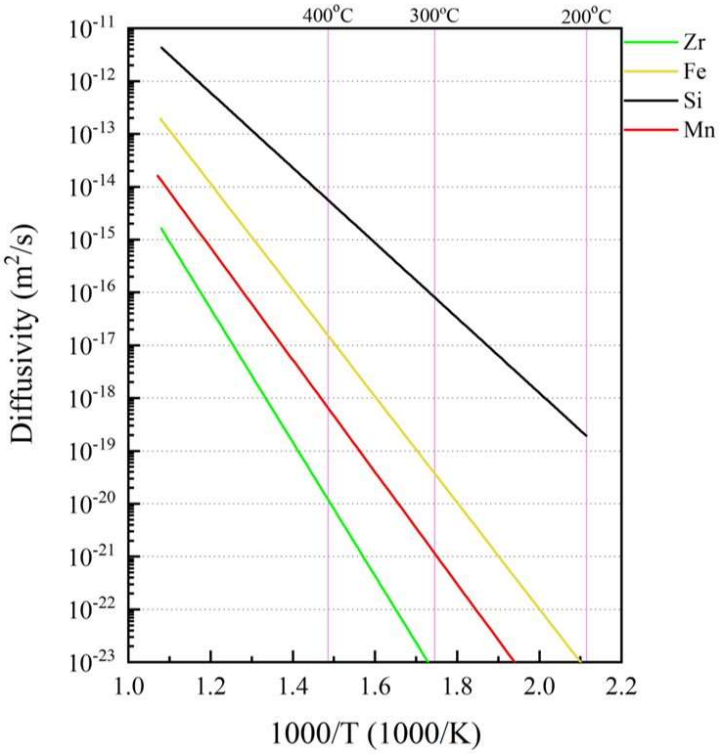

Fig. 12. Diffusivities of alloying elements present in 3003-Zr alloy as a function of the inverse temperature in Kelvin. The functions are plotted based on the data in[39,40]. (For interpretation of the references to color in this figure legend, the reader is referred to the Web version of this article.)

In the present 3003-Zr, heterogenous nucleation of Al_3Zr at the interface between α-Al(Mn,Fe)Si and Al matrix is observed in dendrite periphery regions, as shown in Fig. 8f. This may be induced by the low driving force for precipitation of Al_3Zr disperoids due the lower supersaturation level of Zr in this region. However, the density

of α-dispersoid is much lower by at least one order of magnitude than Al_3Zr in 3003-Zr. Therefore, heterogenous nucleation can hardly exert significant influence on the strengthening effect.

4.2 Thermal stability of dispersoids at 400°C

During isothermal aging at 400°C, 3003-Zr exhibits a significantly higher thermal stability than 3003 alloy, as seen in Fig. 7 and 10. This should be mainly attributed to the continuous formation of high-density nano-sized Al_3Zr dispersoids when α-dispersoids coarsen quickly during aging at 400°C (Fig. 8). The distinct discrepancy in resistance to coarsening between α-Al(Mn,Fe)Si and Al_3Zr dispersoids is determined by the fact that the diffusion constant of Zr in Al ($1.2\times10^{-20}m^2/s$) is an order of magnitude lower than that of Mn ($6.4\times10^{-19}m^2/s$) at 400°C. However, it has to be mentioned that solute Si element, with high concentration in the Al matrix, was reported to accelerate the coarsening of Al_3Zr in Al-Zr alloys at over-aged state[41]. Here, it looks that Si content in the 3003-Zr did not cause fast coarsening of Al_3Zr dispersoids. This is because most of the Si content in the alloy is occupied by α-Al(Mn,Fe)Si dispersoids and constituent particles[30].

4.3 Strengthening effect from two kinds of dispersoids

The application of Mn or Zr as precipitation strengthening element is usually restricted by the limited strengthening efficiency. In the present study, it shows that an enhanced dispersion-hardening can be achieved by two different types of nano dispersoids, α-Al(Mn,Fe)Si and Al_3Zr. The yield strength of 3003-Zr alloy at the peak aged state is even close to the sum of the reference 3003 alloy and the Al-Zr binary

alloy. The significant improvement of dispersion strengthening in this alloy is obviously due to the increase in total density and volume fraction of dispersoids. Another important reason is the improved global distribution of dispersoids across dendrite arms and grains. It is known that for 3xxx alloys with coarse dendrite arms, the distribution of dispersoids is rather in-homogeneous, having a much lower density in the center region of dendrite arms due to the segregation mode of Mn. The precipitation of high density Al_3Zr dispersoids in the dendrite center regions of 3003Zr alloy has significantly improved the global distribution. Regarding the interaction between dislocations and particles in the Orowan mechanism[42], the average size and interparticle spacing of the particles are essential to the strengthening effectiveness. It has been identified in Fig. 4 and 5 that a finer average size and a higher number density of dispersed hardening particles, as well as a decreased interparticle spacing are obtained in the 3003-Zr alloy compared with either the 3003 or binary Al-Zr alloy. As a result, the peak-aged hardness value of 3003-Zr reached to 60.5 with a ΔHV of 12.2 during ramp heating, while a similar peak hardness of 59.3 is obtained during isothermal aging at 400ºC.

Table 3. Reported microhardness and hardness increment (ΔHV) at peak-aged state for some 3xxx and 1xxx Al alloys by different methods, which could be compare with the studied 3003-Zr alloy. For some specific alloys hardness values after aging at 400 for about 250h are marked. Note all the alloys composition are given in the form of wt. %.

Alloy composition (wt. %)	Aging method	Hardness (peak-aged state)	ΔHV (peak-aged state)	Hardness (400ºC/~250h)	Ref.
Al-1.24Mn-0.25Si-0.6Fe-1Mg	Isothermal	55.9	5.4	-	[43]
Al-1.2Mn-0.25Si-0.6Fe-1.1Mg	Isothermal	62.5	7.4	-	[19]
Al-1.19Mn-0.25Si-0.57Fe-1Mg-0.29Sc-0.17Zr	Isothermal	87.6	10.1	-	[5]
Al-1.1Mn-0.18Si-0.5Fe-0.21Cd	Ramp-heating	49.5	8.7	-	[20]

Al-0.97Mn-0.15Si-0.5Fe	Isothermal	43.8	5.4	-	[18]
Al-0.1Sc-0.2Zr-0.15Er	Isothermal	47	25	42.3	[44]
Al-0.03Sc-0.28Zr-0.03Er-0.1Si	Isothermal	58.6	33	53.5	[45]
Al-0.03Sc-0.28Zr-0.03Er-0.1Si	Isochronal	57.9	32.3	-	[46]
Al-0.02Sc-0.28Zr-0.03Er-0.1Si-0.81Mn-0.28Mo	Isothermal	67.2	31.6	65.6	[30]
Al-0.02Sc-0.28Zr-0.03Er-0.1Si-0.81Mn-0.28Mo-0.02Fe	Isothermal	61.8	26.2	60.5	[30]
Al-0.03Sc-0.28Zr-0.03Er-0.1Si-0.51Mn	Isothermal	62.2	31	59.1	[31]

Table. 3 represents the reported hardness and ΔHV at peak-aged state for several 3xxx and 1xxx Al alloys. Obviously, the peak hardness value of 3003-Zr is much higher than most of the reported 3003 series alloys, even almost equivalent to some Mg-containing 3004 alloy[19]. Particularly, the corresponding ΔHV is even higher than that of 3004 alloy with Sc and Zr additions [5], thus suggesting a better precipitation strengthening effect in the present alloy. On the other hand, 3003-Zr owns a superior peak-aged (12h) and over-aged (250h) HV during isothermal aging at 400ºC, which is comparable to the newly developed Al-0.03Sc-0.28Zr-0.03Er-0.1Si[50], Al-0.02Sc-0.28Zr-0.03Er-0.1Si-0.81Mn-0.28Mo-0.02Fe[30] and Al-0.03Sc-0.28Zr-0.03Er-0.1Si-0.51Mn [31] alloys. Considering the improved dispersion-hardening effect, good thermal stability, low price and simple aging regimes without any homogenization or solution treatment in the 3003-Zr, the present study can serve as an effective method to design low-cost heat-resistant Al alloys in massive production.

5. Conclusion

In this work, 0.28wt% Zr was added into a commercial 3003 alloy, resulting in a concurrent precipitation of nanoscale α-Al(Mn,Fe)Si and Al_3Zr dispersoids upon aging.

A systematic investigation on the as-cast microstructure, precipitation behavior, and thermal stability of dispersoids, and mechanical properties has been done. The following conclusions can be drawn:

(1) High density nano-sized dispersoids of both α-Al(Mn,Fe)Si and Al_3Zr are obtained in 3003-Zr alloy by a ramp heating. The precipitation of high density Al_3Zr dispersoids in the dendrite center region significantly improve the homogeneity of the dispersoids distribution across dendrite arms and grains.

(2) Compared with the binary Al-Zr alloy, the precipitation kinetics of Al_3Zr is significantly promoted in 3003-Zr which results in a finer mean radius of 2.4nm at peak age state during ramp heating.

(3) A distinct improved yield strength of 99MPa is achieved in 3003-Zr alloy during ramp heating, which is much higher than that of reference 3003 alloy (69MPa) and Al-Zr binary alloy (36MPa).

(4) 3003-Zr exhibits an excellent heat-resistance with a stable yield strength from 12h (106MPa) up to 250h (107MPa) during isothermal aging at 400^{o}C. This is because that the strength increment from further precipitation of Al_3Zr can compensate the strength reduction due to the fast coarsening of α-dispersoid.

Author contributions

Shiwei Pan: Investigation, Analysis, Writing - original draft, **Feng Qian**: Investigation, **Chunan Li**: Analysis, Writing - review &editing, **Jiawei Yang**: Investigation, **Zidong Wang**: Supervision, **Yanjun Li**: Conceptualization, Supervision, Writing - review & editing, Funding acquisition.

Data availability

The raw/processed data required to reproduce these findings cannot be shared at this time as the data also forms part of an ongoing study.

Acknowledgment

The authors would like to acknowledge the Norwegian Center for Transmission Electron Microscopy (NORTEM) and Electron Microscopy Lab (EM Lab) at NTNU for the characterization work. Shiwei Pan would like to acknowledge the China Scholarship Council ("State Scholarship Fund", No. 201906460095) for the scholarship granted to support this work. Dr. Di Wan is greatly acknowledged for his guidance on high-magnification SEM operations.

References

[1] J.D. Robson, O. Engler, C. Sigli, A. Deschamps, W.J. Poole, Advances in Microstructural Understanding of Wrought Aluminum Alloys, Metallurgical and Materials Transactions A: Physical Metallurgy and Materials Science. 51 (2020) 4377–4389. https://doi.org/10.1007/s11661-020-05908-9.

[2] F. Qian, E.A. Mørtsell, C.D. Marioara, S.J. Andersen, Y. Li, Improving ageing kinetics and precipitation hardening in an Al-Mg-Si alloy by minor Cd addition, Materialia. 4 (2018) 33–37. https://doi.org/10.1016/j.mtla.2018.09.006.

[3] J.D. Poplawsky, B.K. Milligan, L.F. Allard, D. Shin, P. Shower, M.F. Chisholm, A. Shyam, The synergistic role of Mn and Zr/Ti in producing θ′/L12 co-precipitates in Al-Cu alloys, Acta Materialia. 194 (2020) 577–586. https://doi.org/10.1016/j.actamat.2020.05.043.

[4] S. Pan, X. Chen, X. Zhou, Z. Wang, K. Chen, Y. Cao, F. Lu, S. Li, Micro-alloying effect of Er and Zr on microstructural evolution and yield strength of Al-3Cu (wt.%) binary alloys, Materials Science and Engineering A. 790 (2020). https://doi.org/10.1016/j.msea.2020.139391.

[5] Z. Li, Z. Zhang, X.G. Chen, Improvement in the mechanical properties and creep resistance of Al-Mn-Mg 3004 alloy with Sc and Zr addition, Materials Science and Engineering A. 729 (2018) 196–207. https://doi.org/10.1016/j.msea.2018.05.055.

[6] A.R. Farkoosh, X. Grant Chen, M. Pekguleryuz, Interaction between molybdenum and manganese to form effective dispersoids in an Al-Si-Cu-Mg alloy and their influence on creep resistance, Materials Science and Engineering A. 627 (2015) 127–138. https://doi.org/10.1016/j.msea.2014.12.115.

[7] J.D. Robson, P.B. Prangnell, Dispersoid precipitation and process modelling in zirconium containing commercial aluminum alloys, Acta Materialia. 49 (2001) 599–613. https://doi.org/10.1016/S1359-6454(00)00351-7.

[8] R.A. Karnesky, D.C. Dunand, D.N. Seidman, Evolution of nanoscale precipitates in Al microalloyed with Sc and Er, Acta Materialia. 57 (2009) 4022–4031.

https://doi.org/10.1016/j.actamat.2009.04.034.

[9] K.E. Knipling, D.C. Dunand, D.N. Seidman, Criteria for developing castable, creep-resistant aluminum-based alloys - A review, International Journal of Materials Research. 97 (2006) 246–265.

[10] N.A. Belov, N.O. Korotkova, T.K. Akopyan, A.M. Pesin, Phase composition and mechanical properties of Al–1.5%Cu–1.5%Mn–0.35%Zr(Fe,Si) wire alloy, Journal of Alloys and Compounds. 782 (2019) 735–746. https://doi.org/10.1016/j.jallcom.2018.12.240.

[11] T. Dorin, M. Ramajayam, J. Lamb, T. Langan, Effect of Sc and Zr additions on the microstructure/strength of Al-Cu binary alloys, Materials Science and Engineering A. 707 (2017) 58–64. https://doi.org/10.1016/j.msea.2017.09.032.

[12] S. Mondol, S.K. Makineni, S. Kumar, K. Chattopadhyay, Enhancement of High Temperature Strength of 2219 Alloys Through Small Additions of Nb and Zr and a Novel Heat Treatment, Metallurgical and Materials Transactions A: Physical Metallurgy and Materials Science. 49 (2018) 3047–3057. https://doi.org/10.1007/s11661-018-4614-3.

[13] Y.J. Li, L. Arnberg, Quantitative study on the precipitation behavior of dispersoids in DC-cast AA3003 alloy during heating and homogenization, Acta Materialia. 51 (2003) 3415–3428. https://doi.org/10.1016/S1359-6454(03)00160-5.

[14] Y.J. Li, A.M.F. Muggerud, A. Olsen, T. Furu, Precipitation of partially coherent α-Al(Mn,Fe)Si dispersoids and their strengthening effect in AA 3003 alloy, Acta Materialia. 60 (2012) 1004–1014. https://doi.org/10.1016/j.actamat.2011.11.003.

[15] Y.J. Li, W.Z. Zhang, K. Marthinsen, Precipitation crystallography of plate-shaped Al 6(Mn,Fe) dispersoids in AA5182 alloy, Acta Materialia. 60 (2012) 5963–5974. https://doi.org/10.1016/j.actamat.2012.06.022.

[16] A.M.F. Muggerud, Y. Li, R. Holmestad, S.J. Andersen, Mackay icosahedron explaining orientation relationship of dispersoids in aluminium alloys, Acta Crystallographica Section B: Structural Science, Crystal Engineering and Materials. 70 (2014) 888–896. https://doi.org/10.1107/S2052520614017880.

[17] A.M.F. Muggerud, Y. Li, R. Holmestad, Composition and orientation relationships of constituent particles in 3xxx aluminum alloys, Philosophical Magazine. 94 (2014) 556–568. https://doi.org/10.1080/14786435.2013.857796.

[18] A.M.F. Muggerud, E.A. Mørtsell, Y. Li, R. Holmestad, Dispersoid strengthening in AA3xxx alloys with varying Mn and Si content during annealing at low temperatures, Materials Science and Engineering A. 567 (2013) 21–28. https://doi.org/10.1016/j.msea.2013.01.004.

[19] K. Liu, X.G. Chen, Development of Al-Mn-Mg 3004 alloy for applications at elevated temperature via dispersoid strengthening, Materials and Design. 84 (2015) 340–350. https://doi.org/10.1016/j.matdes.2015.06.140.

[20] F. Qian, S. Jin, G. Sha, Y. Li, Enhanced dispersoid precipitation and dispersion strengthening in an Al alloy by microalloying with Cd, Acta Materialia. 157 (2018) 114–125. https://doi.org/10.1016/j.actamat.2018.07.001.

[21] S.P. Wen, K.Y. Gao, Y. Li, H. Huang, Z.R. Nie, Synergetic effect of Er and Zr on the precipitation hardening of Al-Er-Zr alloy, Scripta Materialia. 65 (2011) 592–595. https://doi.org/10.1016/j.scriptamat.2011.06.033.

[22] K.E. Knipling, D.C. Dunand, D.N. Seidman, Nucleation and precipitation strengthening in dilute Al-Ti and Al-Zr alloys, Metallurgical and Materials Transactions A: Physical Metallurgy and Materials Science. 38 (2007) 2552–2563. https://doi.org/10.1007/s11661-007-9283-6.

[23] K.E. Knipling, D.C. Dunand, D.N. Seidman, Precipitation evolution in Al-Zr and Al-Zr-Ti alloys during isothermal aging at 375-425 °C, Acta Materialia. 56 (2008) 114–127. https://doi.org/10.1016/j.actamat.2007.09.004.

[24] N.A. Belov, A.N. Alabin, D.G. Eskin, V. V. Istomin-Kastrovskii, Optimization of hardening of Al-Zr-Sc cast alloys, Journal of Materials Science. 41 (2006) 5890–5899. https://doi.org/10.1007/s10853-006-0265-7.

[25] C.B. Fuller, J.L. Murray, D.N. Seidman, Temporal evolution of the nanostructure of Al(Sc,Zr) alloys: Part i - Chemical compositions of Al3(Sc1-xZrx) precipitates, Acta Materialia. 53 (2005) 5401–5413. https://doi.org/10.1016/j.actamat.2005.08.016.

[26] H. Li, J. Bin, J. Liu, Z. Gao, X. Lu, Precipitation evolution and coarsening resistance at 400°C of Al microalloyed with Zr and Er, Scripta Materialia. 67 (2012) 73–76. https://doi.org/10.1016/j.scriptamat.2012.03.026.

[27] S.P. Wen, K.Y. Gao, H. Huang, W. Wang, Z.R. Nie, Role of Yb and Si on the precipitation hardening and recrystallization of dilute Al-Zr alloys, Journal of Alloys and Compounds. 599 (2014) 65–70. https://doi.org/10.1016/j.jallcom.2014.02.065.

[28] C. Booth-Morrison, Z. Mao, M. Diaz, D.C. Dunand, C. Wolverton, D.N. Seidman, Role of silicon in accelerating the nucleation of Al 3(Sc,Zr) precipitates in dilute Al-Sc-Zr alloys, Acta Materialia. 60 (2012) 4740–4752. https://doi.org/10.1016/j.actamat.2012.05.036.

[29] H. Gao, Y. Wang, J. Wang, B. Sun, D. Apelian, Aging and recrystallization behavior of quaternary Al-0.25Zr-0.03Y-0.10Si alloy, Materials Science & Engineering A. 763 (2019) 138160.

[30] A. de Luca, D.N. Seidman, D.C. Dunand, Effects of Mo and Mn microadditions on strengthening and over-aging resistance of nanoprecipitation-strengthened Al-Zr-Sc-Er-Si alloys, Acta Materialia. 165 (2019) 1–14. https://doi.org/10.1016/j.actamat.2018.11.031.

[31] S. Shu, A. de Luca, D.C. Dunand, D.N. Seidman, Individual and synergistic effects of Mn and Mo micro-additions on precipitation and strengthening of a dilute Al–Zr-Sc-Er-Si alloy, Materials Science and Engineering A. 800 (2021) 140288. https://doi.org/10.1016/j.msea.2020.140288.

[32] A. de Luca, D.N. Seidman, D.C. Dunand, Mn and Mo additions to a dilute Al-Zr-Sc-Er-Si-based alloy to improve creep resistance through solid-solution- and precipitation-strengthening, Acta Materialia. 194 (2020) 60–67. https://doi.org/10.1016/j.actamat.2020.04.022.

[33] ASTM International, ASTM E21–09: standard test method for elevated temperature tension tests of metallic materials, West Conshohocken, PA, 2009. https://doi.org/10.1520/E0021-09.

[34] P. Schumacher, A.L. Greer, J. Worth, P. V. Evans, M.A. Kearns, P. Fisher, A.H.

Green, New studies of nucleation mechanisms in aluminium alloys: Implications for grain refinement practice, Materials Science and Technology. 14 (1998) 394–404. https://doi.org/10.1179/mst.1998.14.5.394.

[35] Y. Wang, C.M. Fang, L. Zhou, T. Hashimoto, X. Zhou, Q.M. Ramasse, Z. Fan, Mechanism for Zr poisoning of Al-Ti-B based grain refiners, Acta Materialia. 164 (2019) 428–439. https://doi.org/10.1016/j.actamat.2018.10.056.

[36] Yanjun. Li, Lars. Arnberg, Precipitation of dispersoids in DC-cast AA3103 alloy during heat treatment, Light Metals. (2003) 1021–1027. https://doi.org/10.1007/978-3-319-48228-6_129.

[37] S. Jiang, H. Wang, Y. Wu, X. Liu, H. Chen, M. Yao, B. Gault, D. Ponge, D. Raabe, A. Hirata, M. Chen, Y. Wang, Z. Lu, Ultrastrong steel via minimal lattice misfit and high-density nanoprecipitation, Nature. 544 (2017) 460–464. https://doi.org/10.1038/nature22032.

[38] T. Gao, A. Ceguerra, A. Breen, X. Liu, Y. Wu, S. Ringer, Precipitation behaviors of cubic and tetragonal Zr-rich phase in Al-(Si-)Zr alloys, Journal of Alloys and Compounds. 674 (2016) 125–130. https://doi.org/10.1016/j.jallcom.2016.02.236.

[39] S. Fujikawa, K. Hirano, Y. Fukushima, Diffusion of silicon in aluminum, Metallurgical Transactions A. 9 (1978) 1811–1815. https://doi.org/10.1007/BF02663412.

[40] Y. Du, Y.A. Chang, B. Huang, W. Gong, Z. Jin, H. Xu, Z. Yuan, Y. Liu, Y. He, F.Y. Xie, Diffusion coefficients of some solutes in fcc and liquid Al: Critical evaluation and correlation, Materials Science and Engineering A. 363 (2003) 140–151. https://doi.org/10.1016/S0921-5093(03)00624-5.

[41] A.R. Farkoosh, D.C. Dunand, D.N. Seidman, Effects of W and Si microadditions on microstructure and the strength of dilute precipitation-strengthened Al–Zr–Er alloys, Materials Science and Engineering A. 798 (2020). https://doi.org/10.1016/j.msea.2020.140159.

[42] S. Queyreau, G. Monnet, B. Devincre, Orowan strengthening and forest hardening superposition examined by dislocation dynamics simulations, Acta

Materialia. 58 (2010) 5586–5595. https://doi.org/10.1016/j.actamat.2010.06.028.

[43] Z. Li, Z. Zhang, X.G. Chen, Microstructure, elevated-temperature mechanical properties and creep resistance of dispersoid-strengthened Al-Mn-Mg 3xxx alloys with varying Mg and Si contents, Materials Science and Engineering A. 708 (2017) 383–394. https://doi.org/10.1016/j.msea.2017.10.013.

[44] C. Booth-Morrison, D.C. Dunand, D.N. Seidman, Coarsening resistance at 400 °c of precipitation-strengthened Al-Zr-Sc-Er alloys, Acta Materialia. 59 (2011) 7029–7042. https://doi.org/10.1016/j.actamat.2011.07.057.

[45] A. de Luca, D.C. Dunand, D.N. Seidman, Microstructure and mechanical properties of a precipitation-strengthened Al-Zr-Sc-Er-Si alloy with a very small Sc content, Acta Materialia. 144 (2018) 80–91. https://doi.org/10.1016/j.actamat.2017.10.040.

[46] A. de Luca, D.C. Dunand, D.N. Seidman, Mechanical properties and optimization of the aging of a dilute Al-Sc-Er-Zr-Si alloy with a high Zr/Sc ratio, Acta Materialia. 119 (2016) 35–42. https://doi.org/10.1016/j.actamat.2016.08.018.